ANTIMICROBIAL AGENTS AND CHEMOTHERAPY, Oct. 2010, p. 4208–4218 Vol. 54, No. 10
0066-4804/10/$12.00 doi:10.1128/AAC.01830-09

Silver Coordination Polymers for Prevention of Implant Infection: Thiol Interaction, Impact on Respiratory Chain Enzymes, and Hydroxyl Radical Induction▽†

Oliver Gordon,[1] Tünde Vig Slenters,[2]‡ Priscilla S. Brunetto,[2] Amer E. Villaruz,[3] Daniel E. Sturdevant,[4] Michael Otto,[3] Regine Landmann,[1]* and Katharina M. Fromm[2]*

Infection Biology, Department of Biomedicine, University Hospital, CH-4056 Basel, Switzerland[1]; University of Fribourg, Department of Chemistry, Chemin du Musée 9, CH-1700 Fribourg, Switzerland[2]; National Institute of Allergy and Infectious Diseases, The National Institutes of Health, Bldg. 33, 1W10, 9000 Rockville Pike, Bethesda, Maryland 20892[3]; and Research Technologies Branch, Genomics Unit, Rocky Mountain Laboratories, National Institute of Allergy and Infectious Diseases, The National Institutes of Health, 903 South 4th Street, Hamilton, Montana 59840[4]

Received 26 December 2009/Returned for modification 3 June 2010/Accepted 21 July 2010

Prosthetic joint replacements are used increasingly to alleviate pain and improve mobility of the progressively older and more obese population. Implant infection occurs in about 5% of patients and entails significant morbidity and high social costs. It is most often caused by staphylococci, which are introduced perioperatively. They are a source of prolonged seeding and difficult to treat due to antibiotic resistance; therefore, infection prevention by prosthesis coating with nonantibiotic-type anti-infective substances is indicated. A renewed interest in topically used silver has fostered development of silver nanoparticles, which, however, present a potential health hazard. Here we present new silver coordination polymer networks with tailored physical and chemical properties as nanostructured coatings on metallic implant substrates. These compounds exhibited strong biofilm sugar-independent bactericidal activity on *in vitro*-grown biofilms and prevented murine *Staphylococcus epidermidis* implant infection *in vivo* with slow release of silver ions and limited transient leukocyte cytotoxicity. Furthermore, we describe the biochemical and molecular mechanisms of silver ion action by gene screening and by targeting cell metabolism of *S. epidermidis* at different levels. We demonstrate that silver ions inactivate enzymes by binding sulfhydryl (thiol) groups in amino acids and promote the release of iron with subsequent hydroxyl radical formation by an indirect mechanism likely mediated by reactive oxygen species. This is the first report investigating the global metabolic effects of silver in the context of a therapeutic application. We anticipate that the compounds presented here open a new treatment field with a high medical impact.

With ageing populations and rising obesity, the number of patients requiring joint replacement or internal fixation devices is steadily increasing. Occurring at a rate of 5%, orthopedic implant infections remain one of the most devastating complications (45). Low-virulence organisms, including *Staphylococcus epidermidis*, are mostly responsible for perioperative infections of implants (50), when bacteria proliferate and cluster in multilayers known as biofilms (15). This structure allows bacteria to resist antimicrobial agents and immune responses (24).

Therefore, early prevention of infection is a major clinical concern. An attractive concept for protection against infection is the entrapment of pharmaceuticals in matrices on and around implant surfaces and their subsequent release by diffusion. With increasing bacterial resistance against antibiotics, silver and its compounds—historically well known for their antimicrobial effect—have come back into the focus of research (9). Silver ions are proposed to react with electron donor groups (N, O, or S atoms), which are present in bacteria as, e.g., amino, imidazole, phosphate, carboxyl, or thiol groups in proteins or in DNA (8). While the interaction with thiol groups seems to play an essential role in bacterial inactivation (27), it is unclear whether this alone explains the uncoupling of the respiratory chain from oxidative phosphorylation and the collapse of the proton motive force (PMF) at the cytoplasmic membrane. Upon exposure to low concentrations of silver ions, an initial increase in respiration was observed, which was considered a compensation for the loss of proton concentration gradient. Yet, silver ions did not increase proton permeability like a traditional uncoupler. Therefore, it was proposed that the loss of PMF was due to protein inactivation, the interaction sites of which were not identified (18).

With the aim of the elaboration of an antimicrobial and biocompatible implant coating, coordination polymer networks based on silver ions have been developed as nanostructured coatings with tunable solubility, light stability, and anti-

* Corresponding author. Present address for Regine Landmann: University of Basel, Klingelbergstrasse 61, 4056 Basel, Switzerland. Phone: 41 61 2652065. Fax: 41 61 2652230. E-mail: regine.landmann@unibas.ch. Mailing address for Katharina M. Fromm: University of Fribourg, Department of Chemistry, Chemin du Musée 9, CH-1700 Fribourg, Switzerland. Phone: 41 263008732. Fax: 41 263009738. E-mail: katharina.fromm@unifr.ch.

† Supplemental material for this article may be found at http://aac.asm.org/.

‡ Present address: University of Basel, Department of Chemistry, St. Johanns-Ring 19, CH-4056 Basel, Switzerland.

▽ Published ahead of print on 26 July 2010.

microbial effect. Here, we identified the molecular site of Ag^+ action and the metabolic consequences leading to bacterial death. First, we found thiol interaction—but not DNA, phosphate, or carboxyl interaction—to be the major reason for the bactericidal activity. Second, we showed immediate inactivation of proteins after exposure to silver ions. Third, we provided evidence for iron leakage by measuring hydroxyl radical formation after Ag^+ treatment. Finally, we analyzed the genome-wide gene regulatory response of *S. epidermidis* to silver treatment and confirmed the detected biochemical effects at the transcriptional level.

MATERIALS AND METHODS

Media and chemical substances. Tryptic soy broth (TSB) and Mueller-Hinton broth and agar (MHB and MHA) were obtained from Becton Dickinson (Allschwil, Switzerland).

Silver nitrate was obtained from Acros Organics (Geel, Belgium). Kanamycin, potassium phosphate (dibasic), cysteine, glutamate, glutathione, thiourea, fluorocitrate, potassium cyanide, phenazine methosulfate (PMS), 2,6-dichloroindophenol (DCPIP), Na succinate, and Na malonate were from Sigma-Aldrich (Buchs, Switzerland), lysostaphin was from Genmedics (Reutlingen, Germany), and 3′-(*p*-hydroxyphenyl) fluorescein (HPF) was from Invitrogen (Lucerne, Switzerland).

Bacterial strains and growth conditions. *S. epidermidis* 1457 bacteria were freshly grown in TSB for 7 h at 37°C without shaking and then diluted 1:100 for an overnight (ON) culture, which was used for the experiments. Bacterial numbers were estimated by determining the optical density at 600 nm and assessed by plating serial dilutions on MHA.

Solubility in water and tissue cage fluid (TCF). For the dissolution studies, the coordination polymer compounds were synthesized in a manner previously described (42). AgCl was prepared fresh by precipitation of a mixture of molar equivalents of concentrated NaCl and $AgNO_3$ aqueous (nanopure water) solutions and subsequently stored in the dark. Five milligrams of compound was treated with 2 ml water or medium and stored in the dark for 24 h. To 0.5 ml of the filtered solution, 0.5 ml of 10% HNO_3 solution was added and diluted to 10 ml with water for silver determination by atomic absorption spectroscopy (AAS). The remaining precipitate was washed three times with ethanol (EtOH) and dried under vacuum, and a powder spectrum was determined in order to monitor chemical changes during dissolution.

Dissolution tests from coated substrates and silver determination on surfaces. Coated substrates were put into individual wells of a crystallization plate and overlaid with the different media for 24 h in the dark. Thereafter, the solution was filtered and diluted 10 to 20 times with water. AAS measurement was carried out to determine the silver concentration of the media after incubation of the substrates. The loading of the substrates/plates was measured by AAS after the complete removal of the coating with 1 to 2 ml of 20% HNO_3 solution and 2 min of sonication.

AAS measurements. The absorption measurements were made by using a Shimadzu AA-6300 device with a combined Au/Ag lamp in an acetylene-air flame without background correction. Diluted HNO_3 was used to keep the silver ions in solution; the concentration of the acid depended on the sample.

Coating of Au(III) plates. Flame-annealed plates were treated in separate closed glass vessels (15 ml). The plates were immersed in 10 ml disulfide solution [5 mM bis 2-((4-pyridinylcarbonyl)oxy)ethyl disulfide dissolved in 100 ml CH_2Cl_2-EtOH (1:1)] for pretreatment. After 5 days of pretreatment, the plate was washed with EtOH and immediately put into 10 ml of $AgNO_3$ plus ligand 1 [L1 = ethanediyl bis(isonicotinate)] ($AgNO_3$+L1) solution, consisting of a mixture of 5 ml 2 mM $AgNO_3$ and 5 ml 2 mM L1 solution. The immersed gold plates were placed in the dark for incubation times ranging from 3 h to 14 days. Then, the plates were removed, washed with EtOH, and dried in the dark under vacuum over P_2O_5. The prepared samples were kept in the dark in a closed, clean container.

Coating of titanium substrates. The titanium substrates were sonicated for 10 min, once in EtOH and three times in distilled water, and dried under vacuum over P_2O_5. Disks, cylinders, or cages were treated in 10 ml of $AgNO_3$+L1 solution. The concentration of the solution varied between 0.5 mM and 2 mM, and the treating time varied between 3 h and 14 days.

Agar inhibition assays. MHA was melted and then cooled down to approximately 50°C. *S. epidermidis* 1457 bacteria were diluted to 1×10^4 CFU/ml to 1×10^7 CFU/ml in the agar. Gold plates and titanium beads were completely covered with this agar. The plates were incubated for 18 h at 37°C, and the inhibition zones around the gold plates and titanium beads were measured.

Foreign-body infection model. The materials used for cages were anodized commercial pure titanium (cpTi; ISO 5832-2) and electropolished and grid-blasted stainless steel (SS; ISO 5832-1). The cylindrical cages (8.5 by 1 by 30 mm; volume, 1.9 ml) have been described elsewhere (49).

Female C57BL/6 mice, 10 to 12 weeks old, with a mean weight ± standard deviation of 29 ± 2 g were kept under specific-pathogen-free conditions in the Animal House of the Department of Biomedicine, University Hospital Basel, according to the regulations of the Swiss veterinary law and with approval of the University Hospital Basel Animal Ethical Committee. Mice were anesthetized via intraperitoneal injection of 100 mg/kg ketamine (Ketalar; Pfizer AG, Zürich, Switzerland) and 20 mg/kg xylazinum (Xylasol; Graeub AG, Bern, Switzerland). Sterile cages were subcutaneously implanted under aseptic conditions into an air pouch made in the back of each mouse (10, 25). Inocula (200 μl) containing approximately 2×10^6 CFU of *S. epidermidis* were injected into the cage percutaneously immediately after implantation. As reported earlier (25, 49), the mice never developed bacteremia and showed no weight change during the study period; i.e., the infection remained localized.

Tissue cage fluid (TCF) samples were collected 2, 6, 9, and 14 days after infection by percutaneous aspiration from mice that had been anesthetized with isoflurane (Isofluran; Abbott, Wiesbaden, Germany). Samples were transferred into sterile microreaction tubes containing 15 μl of 0.9% NaCl and 1.5% EDTA (pH 7.4) to avoid clotting.

The numbers of planktonic bacteria in TCF were determined by plating serial 10-fold dilutions of 50-μl samples on MHA plates, and the numbers of CFU were counted after 24 h of culture at 37°C. Following sterile explantation, cages were incubated in TSB for 48 h at 37°C. If no CFU were detectable after plating the samples on MHA, the infection was considered cured.

Leukocyte number and viability were assessed by trypan blue exclusion. Leukocyte differentiation in TCF was performed by staining cytospin preparations after loading 1×10^5 cells/100 μl in phosphate-buffered saline (PBS) with 10% fetal calf serum as previously described (26) (Diff-Quick; Dade Behring, Düdingen, Switzerland). Cells were examined under high-power light microscopy.

Time-dependent killing assays. The different substances were added to Falcon tubes in a total volume of 2 ml TSB. Afterwards, each tube was inoculated with 1×10^5 CFU/ml of *S. epidermidis* 1457 and incubated at 37°C without shaking. Bacterial numbers were assessed after 2 h and 4 h by plating serial dilutions on MHA.

Enzyme activity measurements. A modified version of the method described by Nordlie and Arion (32) was used for succinate dehydrogenase (SDH); for aconitase, we modified the method of Sadykov et al. (40). For lysate preparation, *S. epidermidis* bacteria were diluted 1:76 in fresh TSB and grown with shaking to late log phase. After being harvested, supernatants were discarded and bacteria were incubated for 10 min in 750 μl buffer containing 90 mM Tris-HCl (pH 8.0), 100 μM fluorocitrate, and 50 U/ml lysostaphin for aconitase measurement. For SDH measurement, bacteria were resuspended in 750 μl 90 mM Tris-HCl (pH 8.0). Cells were mechanically disrupted using a FastPrep FP120 instrument with the lysing matrix B (MP Biomedicals).

For SDH measurement, cuvettes were prepared containing 20 mM potassium phosphate (pH 7.5), 0.1% Triton X-100, 1 mM KCN, 0.1% PMS, 10 mM Na succinate, and 25 μM DCPIP. The reference cuvettes additionally received a 10 mM concentration of the specific SDH inhibitor Na malonate. The lysate, and eventually also 0.06 mM glutathione and/or $AgNO_3$, was added immediately before measurement. The reduction of DCPIP was simultaneously measured at 600 nm for 2 min in the reference and sample cuvettes to specifically record the activity of SDH (Hitachi U-2810 spectrophotometer). One unit of SDH was defined as an absorbance decrease of $0.0057\ A_{600}$ units per minute, which corresponds to the reduction of 1 nmol of DCPIP.

For aconitase measurement, the lysate was centrifuged at maximum speed for 4 min at 4°C. Cuvettes were prepared containing 90 mM Tris-HCl (pH 8.0). The sample cuvette additionally contained 40 mM isocitric acid. The lysate, and eventually 0.06 mM glutathione and/or $AgNO_3$, was added immediately before measurement. The formation of *cis*-aconitate was simultaneously measured at 240 nm for 10 min in the reference and sample cuvettes. One unit of aconitase was defined as the amount of enzyme that gave a change of $0.0033\ A_{240}$ units per minute.

Protein concentrations were determined with the Pierce BCA protein assay kit (Thermo Scientific) according to the manufacturer's manual, and specific activity was expressed as enzyme units per milligram of protein.

Hydroxyl radical detection. *S. epidermidis* 1457 bacteria were diluted 1:100 in fresh TSB and incubated at 37°C shaking at 230 rpm. Hydroxyl radicals were detected by using the fluorescent reporter dye 3′-(*p*-hydroxyphenyl) fluorescein

(HPF) (41). After reaching early exponential phase, the cultures were supplemented with 10 μM HPF and 0.12 mM $AgNO_3$ or 0.04 mM kanamycin. Glutathione was used in equimolar amounts and thiourea at 150 mM. Tubes were protected from light and again incubated for 2 h under the same conditions. For flow cytometry, cells were collected, washed, and resuspended in 1× PBS. All data were collected using a Beckman Coulter CyAn ADP flow cytometer with a 488-nm argon laser and a 515/545-nm emission filter at a low flow rate.

Iron concentration measurements. Bacterial lysate was prepared as described above for succinate dehydrogenase activity measurements. Samples were either left untreated or supplemented with 0.12 mM $AgNO_3$. As a positive control, lysates were digested with 100 μg/ml proteinase K for 1 h at 37°C and subsequently heated to 98°C for 10 min. After treatment, samples were centrifuged at 13,000 × *g* for 20 min at 4°C. Iron was determined in 100 μl of the centrifuged lysate by inductively coupled plasma mass spectrometry (ICP-MS) on an Agilent 7500cx system equipped with an Octopole reaction system (ORS). The measurements were done using a radio frequency power of 1,500 W, a carrier gas flow of 0.79 liters/min, and a makeup gas flow of 0.30 liters/min at a sample depth of 8 mm. Iron was determined at *m*/*z* 56 in collision mode with an optimized helium flow of 5 ml/min. Indium served as the internal standard.

Gene expression analysis. The ON culture was diluted 1:10 in fresh TSB and incubated for 3 h at 37°C shaking at 230 rpm. This was the 0-min time point, when 20 μg/ml $AgNO_3$ was added and the bacteria were again incubated under the same conditions for 30 min or 90 min. Total RNA was obtained using the RNeasy minikit (Qiagen) and RNAprotect bacterial reagent (Qiagen) according to the manufacturer's instructions. Samples were treated with RNase-free DNase (Qiagen) to rule out the presence of DNA. The RNA concentration was estimated using an ND-1000 spectrophotometer (NanoDrop). The absence of DNA was ensured by random PCR, and RNA quality was evaluated by using control gels and a model 2100 Bioanalyzer (Agilent Technologies).

The 15 samples (3 untreated for 0 min, 3 untreated for 30 min, 3 untreated for 90 min, 3 Ag treated for 30 min, and 3 Ag treated for 90 min) were combined with 2× hybridization buffer, 3 nM B2 control oligonucleotide (Affymetrix 900457), 20× spike-in (Affymetrix 51214), dimethyl sulfoxide (DMSO), and nuclease-free water to achieve a final volume of 200 μl for the 15 individual hybridizations to the custom Affymetrix GeneChip microarray (catalog no. RMLchip3a520351) containing roughly 3,131 *Staphylococcus epidermidis* (SEA, SER) probe sets based on the genomes of *S. epidermidis* strains ATCC 12228 and RP62A (47, 48). The hybridization cocktail, including the components listed above, was transferred into the chip and hybridized at a constant temperature of 40°C for approximately 16 h using the 500k Affymetrix 640 hybridization oven.

Upon completion of the hybridization, each chip was filled with 200 μl of wash buffer A and processed in the Affymetrix Fluidics Station 450. The reagents for the stain mixture consisted of 2× morpholineethanesulfonic acid (MES) stain buffer, 50 mg/ml of bovine serum albumin (BSA), 1 mg/ml of streptavidin phycoerythrin, and water to make up a total volume of 600 μl. Once the staining was complete, the stain reagent was removed and replaced with a holding buffer to make up a total volume of 600 μl for storage and scanning. Upon completion of the fluidics process, each chip was scanned using the Affymetrix 7Gplus GeneChip scanner.

GeneChip Operating Software (GCOS v1.4) was then used to convert the image files to cell intensity data files. All cell intensity data files were normalized by using the scaling method within GCOS and a scaled target of 1250 to produce the analyzed files along with the report files and a pivot table for export into other software.

The expected signal gradient produced from the Affymetrix 20× spike-in hybridization was controlled with *creX*, *bioD*, *bioC*, and *bioB* at 100, 25, 5, and 1.5 pM concentrations, respectively. Quality control methods based upon the magnitude of the total number of genes present (above background signal) and the magnitude of the scale factor (multiplier), required for achieving the same trimmed mean for every sample, revealed no outliers.

The cell intensity data files were input into Partek Genomics Suite software (Partek, Inc., St. Louis, MO; v6.4 6090330) and quantile normalized to produce the principal components analysis (PCA). An analysis of variance (ANOVA) was performed within Partek to compare all samples in order to obtain multiple-test corrected *P* values using the false discovery rate method (4) and was combined with fold change values, signal confidence (above background), and call consistency (as a percent) calculated using custom Excel templates. Genes which had a fold change of at least 2 at a *P* value of <0.05 were considered differently expressed.

Microarray results were verified by reverse transcription (RT)-PCR of the genes *radA*, *recA*, *sdhC*, and *icaB*.

Statistical analysis. Besides the microarray analysis (see previous section), data were analyzed with Prism 5.0a (GraphPad Software, Inc.) and the Mann-Whitney test was used for statistical analyses.

RESULTS

Physical and chemical properties, deposition, and coating analysis of the silver coordination polymer compounds. Coordination polymer networks are a class of compounds situating themselves between polymers and molecular compounds in terms of solubility in aqueous solutions. These networks are generally made of metal ions as nodes and organic molecules, which act as bridging ligands between the nodes (2, 13, 35). For the design of silver coordination polymers, we chose a ligand system L_n [for $n = 1$, L1 = ethanediyl bis(isonicotinate)] (Fig. 1a) derived from two biocompatible components, isonicotinic acid and polyethylene glycol (PEG) units (42), which was neither toxic toward fibroblast or osteoblast cell lines nor antimicrobial against bacteria or yeasts (data not shown). We tested the light stability, solubility, and toxicity of different, previously characterized silver coordination polymers based on L_n and identified $[Ag(L1)NO_3]_n$, compound 1, as most suitable for the proposed application (36–38). Indeed, compound 1 proved stable and did not degrade when exposed to light for longer time scales due to its long Ag-Ag contacts.

Compound 1 was designed to possess a low solubility in aqueous media. Indeed, its solubilities in water and in biological fluid surrounding a model implant in mice (tissue cage fluid [TCF]) were similar and significantly lower than that of $AgNO_3$ in both media (Table 1). AgCl, which is very insoluble in water, had a solubility similar to that of compound 1 in TCF. This was due to the presence of N-donor-containing molecules, which are able to solubilize AgCl in general and to enter into competition with L1 of compound 1, which is also an N donor. Compound 1 was thus the least soluble in TCF compared to AgCl and $AgNO_3$ and also possessed the lowest solubility and best light stability compared to other silver coordination networks tested in our series. Therefore, we selected compound 1 to study deposition on implant materials. Rough and smooth titanium (19), as well as steel, which are both utilized in implants, were used as substrates for the deposition of compound 1. In addition, compound 1 was deposited on oriented gold monolayer Au(III) on glass as a smoother model surface. Coating of Au(III) with compound 1 required pretreatment of the gold surface with an anchor molecule, L′S, provided by cleavage of L′SSL′ in the presence of the Au(III) surface (Fig. 1b). The importance of the disulfide L′SSL′ in the case of Au(III) was proven by comparison with a coating obtained without linker (data not shown). The latter coating showed more inhomogeneities, was less stable, and could be washed off more easily from the surface than that in the presence of the L′S linker. In contrast, compound 1 adhered efficiently to titanium with or without linker molecule, while deposition on steel was always irregular and unstable, independent of the deposition conditions. In all cases, powder X-ray analyses as well as X-ray photoelectron spectroscopy (XPS) (data not shown) of the coatings confirmed the identity of the depot as compound 1.

The deposition conditions which gave the most efficient results in antimicrobial activity were 1 mM for 3 h for Au(III) and 2 mM for 72 h for titanium. Upon loading with 2 mM

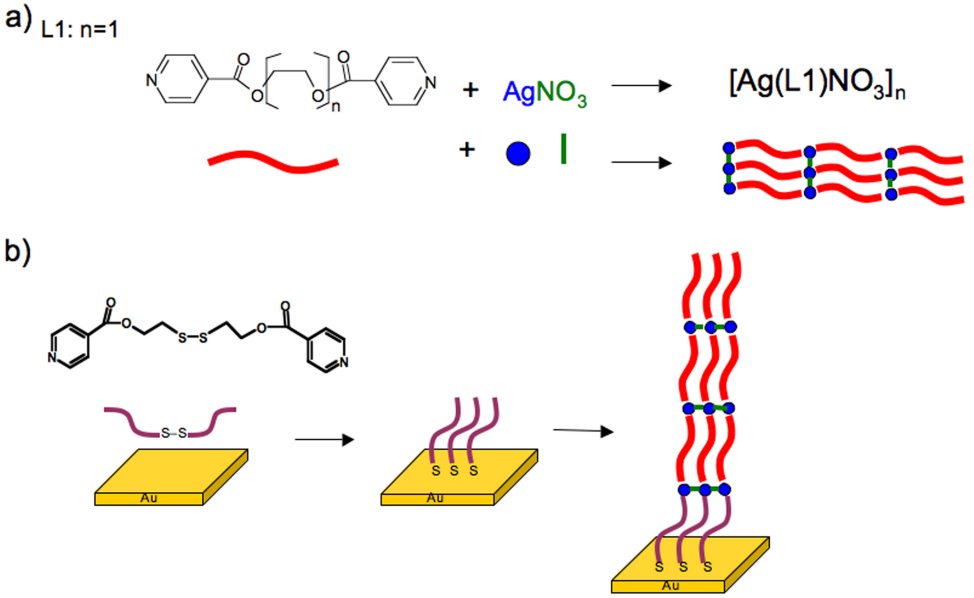

FIG. 1. Synthesis and surface treatment with the silver coordination compound. Compound 1 [$Ag(L1)NO_3$] formation (a) and deposition on Au(III) gold plates (b).

solutions and longer exposure times, larger structures (10- to 1,000-μm crystals of compound 1) were observed on the surface in addition to the nanostructures (data not shown). The most effective loading on Au(III) was roughly 10^{-8} mol/cm^2 of Ag^+, while the corresponding value on titanium was slightly higher (2×10^{-8} mol/cm^2). *In vivo* experiments with titanium cages proved that after a 15-day implantation, silver still remained on the surface at concentrations of at least 2×10^{-10} to 10×10^{-10} mol/cm^2.

Microbicidal activity and toxicity of coordinated silver compounds *in vitro* and *in vivo*. Infections of implants are in 50% of the cases due to staphylococci (50). Therefore, the antimicrobial activity of the coordination compound 1 was tested against *S. epidermidis in vitro*. Agar inhibition assays showed that compound 1 is bactericidal in a dose-dependent manner, both when coated on gold (Fig. 2a) and when coated on titanium (Fig. 2b). Coating on titanium yielded a slightly higher bactericidal activity. Similar data obtained for *S. aureus* are not shown. The bactericidal activity of compound 1 on either substrate was not modified by the presence or absence of polysaccharide intercellular adhesin (PIA), as shown with isogenic *Staphylococcus aureus* and *S. epidermidis* mutants deficient in PIA synthesis (data not shown).

The bactericidal activity was monitored in mice in the subcutaneously implanted titanium cages, which had been coated

TABLE 1. Solubility of different silver compounds in water and tissue cage fluid

Medium	Solubility (mM/liter) of indicated compound in water		
	Compound 1	$AgNO_3$	AgCl
H_2O	0.8	15	0.01
Tissue cage fluid	0.78	5.73	0.9

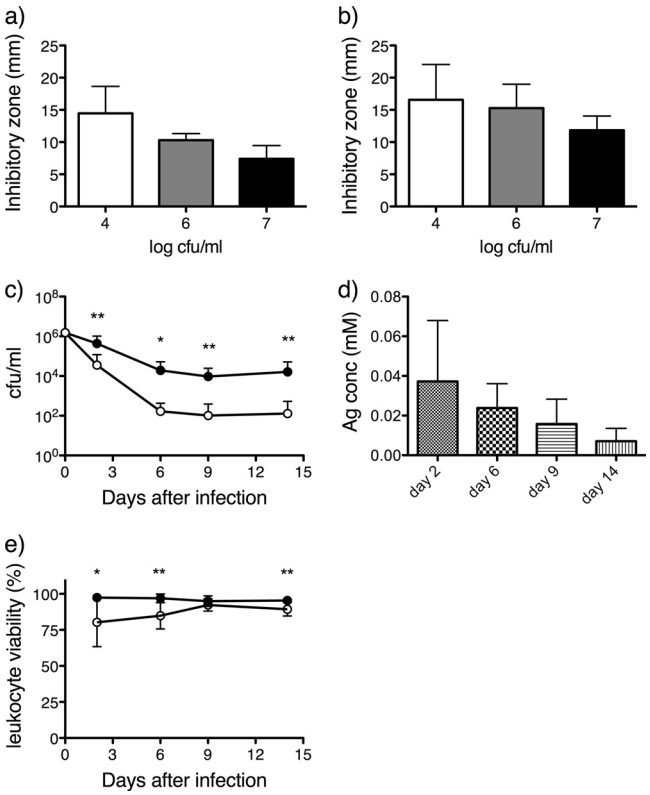

FIG. 2. Agar inhibition assay with *S. epidermidis* 1457 at 10^4 to 10^7 CFU/ml. (a and b) Effects of gold plates coated with 2 mM Ag coordination compound (a) and of titanium beads coated with 5 mM Ag coordination compound (b). (c) Bacterial load in tissue cages (untreated, filled symbols; 1 mM Ag treated, empty symbols) after infection with 2×10^6 CFU *S. epidermidis*. (d) Silver concentration in mM. (e) Viability of leukocytes in tissue cages. Significant differences are indicated (*, $P < 0.05$; **, $P < 0.01$).

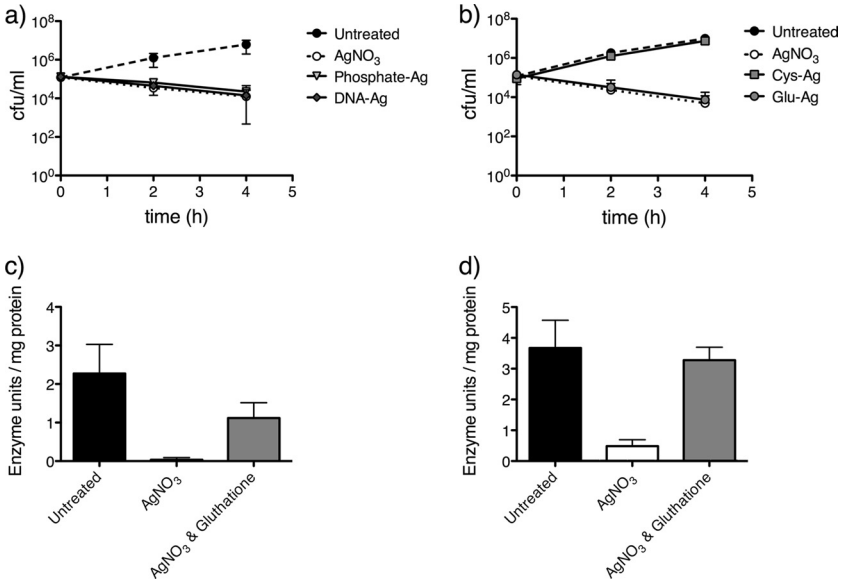

FIG. 3. (a and b) Kill curve of *S. epidermidis* 1457 over 4 h in the presence of 0.12 mM $AgNO_3$ and equimolar phosphate or excess DNA concentrations (a) or equimolar amounts of the thiol group-containing amino acid cysteine or the carboxyl group-containing amino acid glutamate (b). (c and d) Activity measurements of the respiratory chain enzyme succinate dehydrogenase (c) or the TCA cycle enzyme aconitase (d) after addition of 0.06 mM $AgNO_3$ or $AgNO_3$ and an equimolar amount of the cysteine containing tripeptide glutathione.

with compound 1 and inoculated with different numbers of *S. epidermidis* 1457 bacteria. When the mice were infected with low inocula mimicking perioperative infection (5×10^4 CFU), the concentration of planktonic bacteria decreased more rapidly in coated than in uncoated cages, with complete clearance within 6 days for both conditions. At this time, the infection, assessed as growth of adherent bacteria from extracted cages, was completely cured in 67% of coated cages compared to 17% of uncoated cages ($P < 0.05$). For high inocula of 2×10^6 CFU, the decline of planktonic CFU numbers was significantly stronger in coated than in uncoated cages (Fig. 2c). Adherent bacteria remained in 44% of mice with silver-coated cages and in 78% of mice with noncoated cages ($P < 0.05$). Similar data were obtained by inoculation of 2×10^6 CFU of an isogenic mutant deficient in PIA synthesis (data not shown). The silver concentration in TCF on day 2 was similar to the MIC of silver for *S. epidermidis* (0.06 mM). The release of silver ions from the coated cages into the tissue cage fluid corresponded to a fraction of ca. 15% of the total depot after 2 days, a process which slowed down to 3 to 4% after 14 days (Fig. 2d). Tissue cage leukocytes were not massively damaged during this period, since the fraction of viable cells remained above 75% and recovered to over 90% by day 15 (Fig. 2e). The silver-induced leukocyte death was considered moderate compared to the one caused by *S. aureus* infection, for which we had observed a continuously increasing proportion of dead leukocytes during persistent infection (25, 26). In addition, the toxic silver effect disappeared with the cure of the infection and the lessening of silver released from the compound.

Molecular mechanism of silver action. In the past, several targets, including DNA and RNA, as well as phosphate and carboxyl, amino, and thiol groups of amino acids, were reported to bind silver (8). In order to estimate the relative affinities of these reported binding sites for Ag^+ and to evaluate the relevance of the potential targets for the bactericidal effect, time-kill curves in the presence of DNA, phosphate, or the amino acids cysteine or glutamate were established. The addition of an equimolar amount of potassium phosphate and excess DNA did not reduce the antimicrobial activity of silver (Fig. 3a). In contrast, equimolar amounts of the thiol group containing the amino acid cysteine, but not of other amino acids like glutamate, which lacks sulfur, abolished the bactericidal activity (Fig. 3b). In conclusion, our data indicated that interaction with thiol groups, but not with other speculated silver targets, is responsible for its bactericidal activity.

Next we asked if Ag^+ binding of thiol groups interferes with protein function. Therefore, we measured the activity of succinate dehydrogenase (SDH) from the respiratory chain and aconitase from the tricarboxylic acid (TCA) cycle in a crude lysate of *S. epidermidis*. The addition of 0.06 mM $AgNO_3$ to the lysate immediately abolished protein activity, while an equimolar amount of the cysteine containing tripeptide glutathione preserved protein functionality (Fig. 3c and d). In conclusion, silver interaction with thiol groups immediately inhibits the enzymatic activity of proteins.

Since both succinate dehydrogenase and aconitase contain iron-sulfur clusters, we asked if iron could be liberated upon silver treatment and subsequently promote hydroxyl radical formation by the Fenton reaction. Hydroxyl radicals are highly toxic since they damage proteins, lipids, and most prominently DNA (20) and might thereby also play a role in bacterial inactivation. Therefore, we measured hydroxyl radical formation in *S. epidermidis* with the specific reporter dye HPF. Indeed, hydroxyl radical levels were significantly increased upon silver treatment and could be abolished by the addition of an equimolar amount of the cysteine donor glutathione (Fig. 4a). The bactericidal antibiotic kanamycin, which was reported to induce hydroxyl radical formation (22), was used as a positive

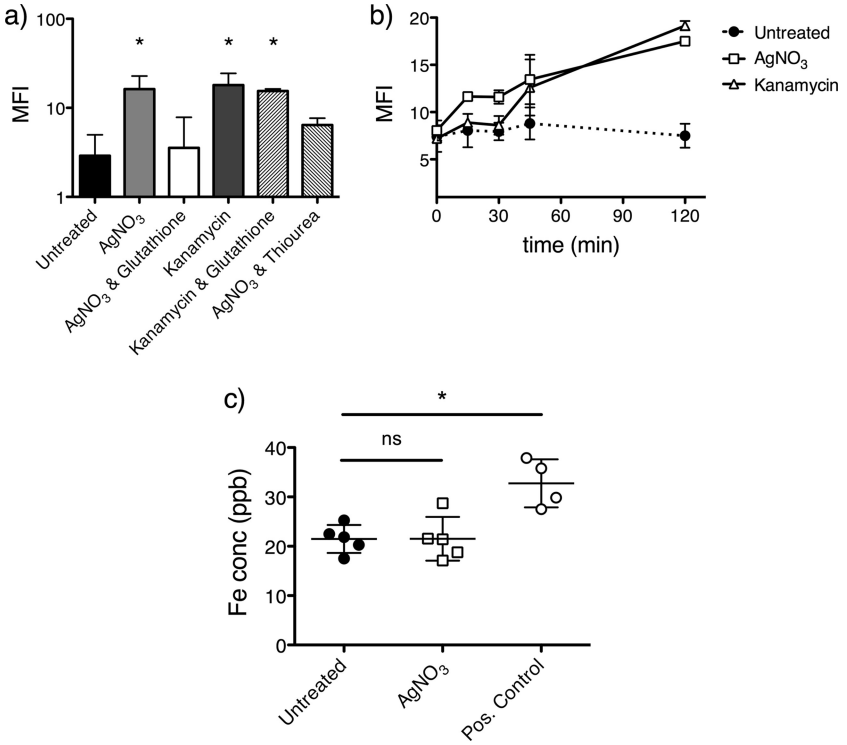

FIG. 4. (a and b) Hydroxyl radical formation in *S. epidermidis* 1457 detected with the specific reporter dye HPF after 2 h of growth (a) or during 2 h of growth (b) in the presence of the indicated substances. (c) Iron concentrations in *S. epidermidis* 1457 lysates measured by ICP-MS. $AgNO_3$ was used at a concentration of 0.12 mM, kanamycin at 0.04 mM. Glutathione was added in an equimolar amount. The Fenton reaction-specific quencher thiourea was used at a concentration of 150 mM. For the positive control of the iron concentration measurements, lysates were digested with 100 μM proteinase K for 1 h and subsequently heated to 98°C for 10 min. Significant differences of results compared to those for untreated samples are indicated (*, $P < 0.05$).

control. In the case of kanamycin, an equimolar amount of glutathione had no effect on hydroxyl radical formation, proving that direct interaction is required at this concentration level. Addition of the Fenton reaction-specific quencher thiourea, which does not contain SH groups, significantly reduced the formation of hydroxyl radicals, indicating that iron ions are involved in their production. We next compared the kinetics of hydroxyl radical formation induced by silver and by kanamycin. While the latter causes hydroxyl radicals by hyperactivating the respiratory chain (22), we found that respiration was blocked shortly after silver treatment without a preceding hyperactivation. Therefore, we expected a faster kinetic of hydroxyl radical formation by silver than by kanamycin. Indeed, during the first 2 h after treatment, silver induced hydroxyl radical formation earlier than kanamycin (Fig. 4b), indicating a more direct mechanism of iron leakage by silver. ICP-MS measurements in *S. epidermidis* lysates, however, indicated that silver itself is not able to liberate coordinated iron (Fig. 4c). In conclusion, we observed rapid hydroxyl radical formation after silver treatment, which is in all likelihood not due to a direct interaction with iron-sulfur clusters.

To analyze the transcriptional response to respiratory enzyme inactivation and subsequent TCA cycle breakdown, we determined the genome-wide gene regulatory response of *S. epidermidis* to $AgNO_3$ treatment (30 and 90 min) using microarrays. The expression of 1,500 genes was altered at both time points. We focused on 113 genes that were upregulated and 69 genes that were downregulated (>2-fold) (see Table S1 in the supplemental material). A less detailed list than that in Table S1 is included in Table 2. Selected important transcriptional changes observed in the microarray were confirmed by quantitative PCR (*icaB*, *sdhC*, *recA*, *radA*).

We found terminal oxidases such as the quinol oxidase more strongly upregulated after silver treatment than initial oxidases, which were even downregulated in the case of succinate dehydrogenase. This could indicate a mechanism against ROS damage derived from electrons unable to exit from the respiratory chain, which by chance reduce molecular oxygen to reactive intermediates (20).

In accordance with the breakdown of respiration, genes coding for glycolytic enzymes were upregulated. The upregulation of fructokinase and downregulation of pyruvate dehydrogenase pointed toward a transition from oxidative to substrate-level phosphorylation. D-Lactate dehydrogenase was downregulated, whereas L-lactate dehydrogenase was unchanged in expression. Genes coding for TCA cycle enzymes were downregulated upon silver treatment, reflecting a diminished need for reduction equivalents in the absence of respiration, so that the expression pattern of energy metabolism enzymes resembled that of growth under anaerobic conditions (17). This was supported by increased lactate levels in aerobically growing *S. epidermidis* in the presence of subinhibitory silver concentrations after 4 to 6 h (data not shown).

The main iron uptake regulator Fur, which represses genes

TABLE 2. Changes in gene expression upon treatment with 0.12 mM $AgNO_3$

Functional category and ORF	Gene	Annotation	Fold change	
			30 min	90 min
Respiratory chain				
SERP0672	*cydA*	Cytochrome *d* ubiquinol oxidase, subunit I	2.10	2.24
SERP0673	*cydB*	Cytochrome *d* ubiquinol oxidase, subunit II	6.54	4.72
SERP0644	*qoxC*	Quinol oxidase, subunit III		2.03
SERP0643	*qoxD*	Quinol oxidase, subunit IV	4.07	4.95
SERP0084	*nuoF*	NADH dehydrogenase subunit 5		2.45
SERP0731	*sdhA*	Succinate dehydrogenase flavoprotein subunit		−3.29
SERP0732	*sdhB*	Succinate dehydrogenase iron-sulfur subunit	2.73	−2.22
SERP0730	*sdhC*	Succinate dehydrogenase, cytochrome b_{558} subunit	−6.32	−43.87
SERP1708	*atpC*	ATP synthase F1, epsilon subunit	2.04	2.81
SERP1709	*atpD*	F_oF_1 ATP synthase subunit beta		2.65
SERP1710	*atpG*	F_oF_1 ATP synthase subunit gamma		2.02
Glycolysis				
SERP1494		Fructokinase, putative	2.81	5.56
SERP0358	*fruK*	1-Phosphofructokinase		8.09
SERP1261	*pyk*	Pyruvate kinase		3.21
SERP0680	*pdhA*	Pyruvate dehydrogenase complex E1 component, alpha subunit		−2.26
SERP0442	*gapA-1*	Glyceraldehyde 3-phosphate dehydrogenase 1		2.48
SERP1250	*gapA-2*	Glyceraldehyde 3-phosphate dehydrogenase 2	−7.05	−101.20
SERP2087		D-Lactate dehydrogenase	−2.44	−2.53
TCA cycle				
SERP1258	*gltA*	Citrate synthase		−2.34
SERP1387	*fumC*	Fumarate hydratase		−3.46
SERP0921	*acnA*	Aconitate hydratase		−3.86
SERP0985	*sucB*	Dihydrolipoamide acetyltransferase		−4.30
SERP0813	*sucC*	Succinyl-CoA synthetase subunit beta		−4.88
Iron homeostasis				
SERP1120	*fur*	Transcriptional regulator, Fur family	7.87	9.69
SERP2127	*feoA*	FeoA family protein	−6.45	−4.15
SERP2126	*feoB*	Ferrous iron transport protein B	−6.85	−6.18
SERP0292	*sitA*	Possible iron transporter	−42.56	−72.04
SERP0291	*sitB*	Possible iron transporter	−10.92	−14.28
SERP0290	*sitC*	Possible iron transporter	−12.44	−16.47
SERP0293	*sirR*	Iron-dependent repressor	−6.68	−6.45
SERP1431	*ftnA*	Ferritin family protein	2.25	2.22
SERP0522		NifU domain protein	11.82	3.19
SERP0499		NifU domain protein	2.20	2.75
Oxidative stress response				
SERP2194	*gpxA-2*	Glutathione peroxidase	3.95	4.26
SERP0500	*sufB*	FeS assembly protein SufB	3.30	3.84
SERP0151	*hslO*	Chaperonin, 33 kDa	3.24	
SERP0728	*trxA*	Thioredoxin	2.09	2.48
SERP0432	*trxB*	Thioredoxin-disulfide reductase	2.66	2.71
SERP0059	*ahpF*	Alkyl hydroperoxide reductase, F subunit	2.52	2.52
SERP0060	*ahpC*	Alkyl hydroperoxide reductase, C subunit	2.27	2.26
SERP2265		Organic hydroperoxide resistance protein, putative		4.48
Cell wall/biofilm				
SERP0518	*dltA*	D-Alanine–D-alanyl carrier protein ligase	2.60	7.82
SERP0519	*dltB*	DltB protein	2.88	11.64
SERP0520	*dltC*	D-alanine–poly(phosphoribitol) ligase subunit 2	2.54	9.68
SERP0521	*dltD*	DltD protein	4.78	18.31
SERP2293	*icaA*	*N*-Glycosyltransferase PgaC	2.36	8.85
SERP2295	*icaB*	Intercellular adhesion protein B	2.51	8.23
SERP2296	*icaC*	Intercellular adhesion protein C	3.29	9.74
SERP2294	*icaD*	Intercellular adhesion protein D	2.10	8.24
SERP2292	*icaR*	Intercellular adhesion regulator	−2.61	−9.37
SERP1731	*murA2*	UDP-*N*-acetylglucosamine 1-carboxyvinyltransferase	−3.02	−5.33
SERP0405	*murB*	UDP-*N*-acetylenolpyruvoylglucosamine reductase	−3.62	−4.21
SERP0993	*murG*	*N*-Acetylglucosaminyl transferase	−4.00	−2.38
SERP0607	*murE*	UDP-*N*-acetylmuramoylalanyl-D-glutamate-2,6-diaminopimelate ligase	−6.25	−2.97
SERP0746	*pbp1*	Penicillin-binding protein 1	−10.59	−9.71

Continued on following page

TABLE 2—*Continued*

Functional category and ORF	Gene	Annotation	Fold change	
			30 min	90 min
SERP1117	*pbp3*	Penicillin-binding protein 3	−13.49	−9.36
SERP0747	*mraY*	Phospho-*N*-acetylmuramoyl-pentapeptide-transferase	−5.17	−6.41
SERP2533	*yycG*	Sensory box histidine kinase YycG	−5.18	−8.32
SERP1844	*femX*	FemX protein	−5.89	−8.31
SERP0946	*femA*	FemA protein	−7.34	−6.55
SERP0827	*uppS*	Undecaprenyl diphosphate synthase	−12.36	−7.17
SERP2024	*lytS*	Sensor histidine kinase LytS	−2.43	−2.81
SERP2025	*lytR*	Response regulator LytR	−9.01	−6.23
SERP2027	*lrgB*	Antiholin-like protein LrgB	−2.97	−26.02
SERP2026	*lrgA*	Murein hydrolase regulator LrgA	−3.86	−71.30
Chaperones/proteases				
SERP0564	*clpB*	ATP-dependent Clp protease, ATP-binding subunit ClpB	7.03	4.37
SERP0165	*clpC*	ATP-dependent Clp protease, ATP-binding subunit ClpC	4.31	3.11
SERP0436	*clpP*	ATP-dependent Clp protease, proteolytic subunit ClpP	6.99	6.12
SERP1238	*clpX*	ATP-dependent protease ATP-binding subunit	2.67	3.38
SERP1484	*groEL*	Chaperonin GroEL	4.46	4.14
SERP1485	*groES*	C-chaperonin GroES	3.02	3.49
SERP1149	*grpE*	Heat shock protein GrpE	2.83	
SERP1147	*dnaJ*	DnaJ protein	3.69	3.18
SERP1148	*dnaK*	DnaK protein	2.57	2.03
SERP0820	*hslU*	ATP-dependent protease ATP-binding subunit	2.28	2.83
SERP0819	*hslV*	ATP-dependent protease peptidase subunit	2.44	3.04
SERP0162	*ctsR*	Transcriptional regulator CtsR	7.40	5.07

involved in iron uptake, if coordinated with intracellular iron (1, 28), was strongly upregulated. Indeed, iron import systems (*sitABC* and *feoAB*) were downregulated after silver treatment. On the other hand, transcription of iron storage proteins like ferritin, as well as expression of NifU domain proteins related to iron-sulfur cluster assembly, were increased after silver treatment.

Several genes involved in the oxidative stress response were upregulated upon silver treatment, indicative of a response to the silver-targeted and damaged thiol-containing antioxidative enzymes.

Silver treatment also yielded an increased transcription of the *icaABCD* operon responsible for PIA synthesis. While genes coding for murein synthesis and assembly were downregulated, the *dltABCD* operon coding for enzymes of teichoic acid (TA) D-alanylation, which has a function in biofilm formation (15), was upregulated. Interestingly, the *lrgAB* operon, coding for an antiholin-like protein, and its positive regulators *lytS* and *lytR* were strongly downregulated upon silver treatment. On the other hand, its antagonist, *cidAB*, and peptidoglycan hydrolases were not changed in expression, indicating enhanced autolytic activity (16, 34). Genes involved in DNA repair were neither clearly up- nor downregulated, but the majority of these genes were enhanced in transcription at the later rather than the earlier time point, suggesting that DNA repair might be triggered even later upon silver treatment. DNA replication and cell division genes were reduced in transcription, which is consistent with the well-described bacteriostatic activity of silver (44). As expected from the demonstrated protein inactivation, genes coding for chaperones, proteases, ribosome constituents, and several amino acid pathways were upregulated after treatment with silver. In conclusion, the genome-wide gene regulatory response of *S. epidermidis* to $AgNO_3$ treatment strengthened our biochemical findings.

DISCUSSION

In the present study, we identified silver coordination compound 1 as a good candidate for microbicidal implant coatings. We elaborated the coating conditions for an optimal bactericidal effect of the compound on model implant surfaces. Furthermore, we demonstrated that the compound has a curative effect upon *S. epidermidis* infection in a murine implant infection model. Moreover, we found that the compound exhibits bactericidal activity toward *S. epidermidis* by a mechanism that involves binding to thiol group-containing amino acids, inactivation of respiratory chain and TCA cycle enzymes, and induction of hydroxyl radical formation. Finally, our results show that *S. epidermidis* responds to these inhibitory influences by a genome-wide adaptive response of altered gene expression.

In the synthesis of compound 1, the use of ligand L was important for tuning the solubility of compound 1 in biological media, guaranteeing a slow silver ion release from the substrates, which is mandatory to avoid pronounced damage to host cells. The immersion time in mother liquor, as well as its concentration, was recognized as a crucial factor for the type of nanostructure of the coating. While short incubation times and low concentrations favored a dense and robust coordination network, longer incubation times and high concentrations promoted formation of brittle aggregates, thereby rendering the silver release in the surrounding tissue less well controllable. In conclusion, compound 1 is a promising candidate for technically easy and fast coating of implants.

S. epidermidis biofilm-associated infection has been studied using multiple models, most frequently by subcutaneous inser-

tion of catheter pieces. Our mouse infection model with tissue cages has several features that optimize relevance for human *S. epidermidis* implant infection (19). The bacteria consist of a floating population in the tissue cage fluid and an adherent population in the biofilm, the former being fed by the turnover of the latter. We found silver particularly effective against adherent bacteria, indicating that the biofilm did not represent a penetration barrier for silver ions. Of note, the presence or absence of PIA had no impact on the bactericidal activity of silver, giving reason to believe that our silver compound has bactericidal activity independent of the chemical composition of the *S. epidermidis* biofilm matrix. Since we showed that thiol groups have the highest affinity for silver ions, proteinaceous biofilm components may potentially offer resistance. However, this is unlikely, as thiol-containing cysteine residues are usually present in their oxidized form in the extracellular milieu. Future experiments with *S. epidermidis* biofilms with mutated proteins such as Aap (39) will address this question. It is commonly accepted that combination regimens are required for implant infections owing to their intrinsic resistance to many antibacterial compounds. Rifampin acting against adherent biofilm-producing staphylococci at the price of rapid resistance and quinolones are the actual treatment of choice, but infection is cleared in only 50% of the cases (50). Thus, as treatment of biofilm-associated infections with antibiotics is difficult in general, prevention of infection e.g., by coating implants, is preferred over treatment. Here we show that nanostructured coordination networks represent optimal coating materials, since they allow a slow, controlled silver release and a protracted effect over 2 weeks, while having only low toxicity on leukocytes. Furthermore, released silver ions act immediately, as shown by blockage of protein activities, which is beneficial for preventing local infections. Possibly the main indication for these compounds will be prevention of perioperative infections. The major effect on imported bacteria can occur immediately and vanishes relatively fast. Thus, long-term bone damage and possible neutralization of Ag^+ effects by extracellular membrane components, which are deposited on implants, may be avoided. Because the bactericidal mechanism of silver targets cysteine residues, which are omnipresent in proteins, silver is effective on a large spectrum of bacteria and target-based mutation to silver resistance is unlikely to develop (7). Accordingly, enterococci, the second class of organisms causing implant infections (50), were also susceptible to $AgNO_3$, as determined by MIC/MBC measurements (data not shown). In summary, the likely broad-spectrum antibiofilm activity and low risk of resistance development render our silver compound a high-potential candidate for clinical application.

In accordance with thiol groups being identified as the main targets of the bactericidal activity of our silver compound, we demonstrated that the enzymes succinate dehydrogenase and aconitase were indeed inactivated immediately after the addition of silver. Respiratory chain enzymes can be considered early, strongly affected targets for silver since they are bound to the cell membrane. In addition, the respiratory chain contains iron, mainly coordinated in iron-sulfur clusters. Since we showed that respiratory chain enzymes are inactivated by silver, we asked if iron might be liberated and subsequently promote hydroxyl radical formation through the Fenton reaction. Indeed, we saw increased hydroxyl radical formation after 2 h of treatment with silver, which was lessened by the addition of thiourea, indicating that the Fenton reaction was involved. Iron-sulfur clusters could be damaged directly by Ag^+, as was shown for copper ions (29). However, Ag^+ most likely did not directly interact with iron-sulfur clusters, since free iron was not significantly increased in Ag^+-treated lysates of staphylococci. Alternatively, cluster inactivation and iron liberation were shown to be a consequence of damage by superoxide anions and hydrogen peroxide (11).

ROS accumulation and subsequent iron leakage may be a consequence of respiratory chain hyperactivation, as proposed for bactericidal antibiotics (22). However, the immediate inactivation of respiratory enzymes by silver excluded a similar mechanism and was reflected by an earlier rise in hydroxyl radical concentration after Ag^+ treatment than after kanamycin treatment. Blockage of respiration is normally followed by decreased ROS formation, since the respiratory chain is the major source (21, 23). Still we postulate that ROS were at the origin of iron-sulfur cluster destruction after Ag^+ treatment. Our argument is supported by previous data showing ROS formation after contact with silver in eukaryotic cells (5). A possible source of ROS might be electrons trapped in the respiratory chain (30, 31), as suggested by the gene upregulation of the terminal and downregulation of the initial respiratory enzymes. Antioxidative enzymes most likely did not detoxify ROS generated from the damaged respiratory chain, since these rely on thiol groups, which became occupied by silver. Thus, even low ROS levels might cause destabilization of oxygen-labile iron sulfur clusters after silver treatment. A further result supporting our hypothesis of compromised antioxidative systems was the upregulation of genes encoding oxidative stress responses.

Of those genes whose expression was differentially regulated in our microarray experiment, most of them were downregulated—some reflecting a general growth arrest, some representing an adaptive response to silver. In *S. epidermidis*, a repression of the TCA cycle indicates not only a transition to substrate-level phosphorylation but also induction of rescue mechanisms like biofilm production (43). Indeed, we observed enhanced transcription of the *ica* genes in our microarray.

Fewer genes were upregulated by silver, most likely those which supported survival. This interpretation holds true for the induction of oxidative stress responses by silver and indicates that ROS formation characterizes its bactericidal effect and has to be antagonized by bacteria. The importance of ROS is also reflected by aerobically grown bacteria being more susceptible to silver than anaerobically grown bacteria (46). Along the same line, the induction of genes involved in iron homeostasis suggests elevated levels of free intracellular iron and an increased need for proteins that bind and coordinate it. This was consistent with the herein-reported hydroxyl radical formation upon silver treatment, which takes place only if free intracellular iron is present. Silver-induced bacterial lysis was reported earlier, although the mechanism underlying this effect remained obscure (6, 14). Our microarray results, however, indicated enhanced autolytic activity as a possible reason. Intriguingly, bacterial holin-like and eukaryotic apoptosis regulatory proteins were described to have striking functional similarities, and the regulation of autolysis was therefore linked to prokaryotic programmed cell death (3, 33). Indeed, a depolar-

ization of the cell membrane and DNA damage due to hydroxyl radical formation might set off a form of programmed cell death in bacteria, in a way similar to apoptosis that was observed in eukaryotic cells after silver treatment (12).

In conclusion, we could successfully prevent implant infection with a compound from which silver was released slowly and reached minimal bactericidal concentrations but caused minimal host cell damage. The design of new ligand systems with different solubilities may render this therapeutic concept tailored to specific implant types.

We found that the bactericidal activity of silver ions is due to key enzyme inactivation by thiol group binding, hydroxyl radical formation, and subsequent DNA damage. The expected rapid de-energization after a sudden block in respiration impedes the induction of efficient rescue mechanisms. In conclusion, a silver-containing coating is very attractive for future infection prevention, since it acts against a broad spectrum of pathogens with a low risk of resistance development.

ACKNOWLEDGMENTS

This study was supported by the Swiss National Science Foundation (grant no. 205320-121813 to K.M.F.), the NCCR Nano, FriMat, and the Intramural Research Program of the National Institute of Allergy and Infectious Disease, U.S. National Institutes of Health (to M.O.).

We are grateful for discussions with Mathias Schmaler and Naja Jann and for the technical help of Zarko Rajacic, Fabrizia Ferracin, and Eline Angevaare. We thank Markus Lenz FHNW North-West Switzerland for the ICP-MS measurements, Reto Luginbühl from Mathys Foundation (Bettlach, Switzerland) for providing titanium and steel substrates, and Greg Somerville (University of Nebraska—Lincoln) for advice with the aconitase assay.

REFERENCES

1. **Bagg, A., and J. B. Neilands.** 1987. Ferric uptake regulation protein acts as a repressor, employing iron (II) as a cofactor to bind the operator of an iron transport operon in Escherichia coli. Biochemistry **26:**5471–5477.
2. **Batten, S. R., S. M. Neville, and D. R. Turner.** 2009. Coordination polymers: design, analysis and application, 1st ed. Royal Society of Chemistry, Cambridge, United Kingdom.
3. **Bayles, K. W.** 2003. Are the molecular strategies that control apoptosis conserved in bacteria? Trends Microbiol. **11:**306–311.
4. **Benjamini, Y. H., and Y. Hochberg.** 1995. Controlling the false discovery rate: a practical and powerful approach to multiple testing. J. Roy. Stat. Soc. **1:**289–300.
5. **Carlson, C., S. M. Hussain, A. M. Schrand, L. K. Braydich-Stolle, K. L. Hess, R. L. Jones, and J. J. Schlager.** 2008. Unique cellular interaction of silver nanoparticles: size-dependent generation of reactive oxygen species. J. Phys. Chem. B **112:**13608–13619.
6. **Chang, Q., H. He, and Z. Ma.** 2008. Efficient disinfection of Escherichia coli in water by silver loaded alumina. J. Inorg. Biochem. **102:**1736–1742.
7. **Chopra, I.** 2007. The increasing use of silver-based products as antimicrobial agents: a useful development or a cause for concern? J. Antimicrob. Chemother. **59:**587–590.
8. **Clement, J. L., and P. S. Jarrett.** 1994. Antibacterial silver. Met. Based Drugs **1:**467–482.
9. **Darouiche, R. O.** 1999. Anti-infective efficacy of silver-coated medical prostheses. Clin. Infect. Dis. **29:**1371–1378.
10. **Dawson, J., C. Rordorf-Adam, T. Geiger, H. Towbin, S. Kunz, H. Nguyen, O. Zingel, D. Chaplin, and K. Vosbeck.** 1993. Interleukin-1 (IL-1) production in a mouse tissue chamber model of inflammation. I. Development and initial characterisation of the model. Agents Actions **38:**247–254.
11. **Flint, D. H., J. F. Tuminello, and M. H. Emptage.** 1993. The inactivation of Fe-S cluster containing hydro-lyases by superoxide. J. Biol. Chem. **268:** 22369–22376.
12. **Foldbjerg, R., P. Olesen, M. Hougaard, D. A. Dang, H. J. Hoffmann, and H. Autrup.** 2009. PVP-coated silver nanoparticles and silver ions induce reactive oxygen species, apoptosis and necrosis in THP-1 monocytes. Toxicol. Lett. **190:**156–162.
13. **Fromm, K. M.** 2008. Coordination polymer networks with s-block metal ions. Coord. Chem. Rev. **252:**856–885.
14. **Gogoi, S. K., P. Gopinath, A. Paul, A. Ramesh, S. S. Ghosh, and A. Chattopadhyay.** 2006. Green fluorescent protein-expressing Escherichia coli as a model system for investigating the antimicrobial activities of silver nanoparticles. Langmuir **22:**9322–9328.
15. **Gotz, F.** 2002. Staphylococcus and biofilms. Mol. Microbiol. **43:**1367–1378.
16. **Groicher, K. H., B. A. Firek, D. F. Fujimoto, and K. W. Bayles.** 2000. The *Staphylococcus aureus lrgAB* operon modulates murein hydrolase activity and penicillin tolerance. J. Bacteriol. **182:**1794–1801.
17. **Hecker, M., A. Reder, S. Fuchs, M. Pagels, and S. Engelmann.** 2009. Physiological proteomics and stress/starvation responses in Bacillus subtilis and Staphylococcus aureus. Res. Microbiol. **160:**245–258.
18. **Holt, K. B., and A. J. Bard.** 2005. Interaction of silver(I) ions with the respiratory chain of Escherichia coli: an electrochemical and scanning electrochemical microscopy study of the antimicrobial mechanism of micromolar Ag^+. Biochemistry **44:**13214–13223.
19. **Hudetz, D., S. Ursic Hudetz, L. G. Harris, R. Luginbuhl, N. F. Friederich, and R. Landmann.** 2008. Weak effect of metal type and ica genes on staphylococcal infection of titanium and stainless steel implants. Clin. Microbiol. Infect. **14:**1135–1145.
20. **Imlay, J. A.** 2003. Pathways of oxidative damage. Annu. Rev. Microbiol. **57:**395–418.
21. **Kadenbach, B., R. Ramzan, L. Wen, and S. Vogt.** 2010. New extension of the Mitchell Theory for oxidative phosphorylation in mitochondria of living organisms. Biochim. Biophys. Acta **1800:**205–212.
22. **Kohanski, M. A., D. J. Dwyer, B. Hayete, C. A. Lawrence, and J. J. Collins.** 2007. A common mechanism of cellular death induced by bactericidal antibiotics. Cell **130:**797–810.
23. **Korshunov, S. S., V. P. Skulachev, and A. A. Starkov.** 1997. High protonic potential actuates a mechanism of production of reactive oxygen species in mitochondria. FEBS Lett. **416:**15–18.
24. **Kristian, S. A., T. A. Birkenstock, U. Sauder, D. Mack, F. Gotz, and R. Landmann.** 2008. Biofilm formation induces C3a release and protects Staphylococcus epidermidis from IgG and complement deposition and from neutrophil-dependent killing. J. Infect. Dis. **197:**1028–1035.
25. **Kristian, S. A., T. Golda, F. Ferracin, S. E. Cramton, B. Neumeister, A. Peschel, F. Gotz, and R. Landmann.** 2004. The ability of biofilm formation does not influence virulence of Staphylococcus aureus and host response in a mouse tissue cage infection model. Microb. Pathog. **36:**237–245.
26. **Kristian, S. A., X. Lauth, V. Nizet, F. Goetz, B. Neumeister, A. Peschel, and R. Landmann.** 2003. Alanylation of teichoic acids protects Staphylococcus aureus against Toll-like receptor 2-dependent host defense in a mouse tissue cage infection model. J. Infect. Dis. **188:**414–423.
27. **Liau, S. Y., D. C. Read, W. J. Pugh, J. R. Furr, and A. D. Russell.** 1997. Interaction of silver nitrate with readily identifiable groups: relationship to the antibacterial action of silver ions. Lett. Appl. Microbiol. **25:**279–283.
28. **Litwin, C. M., S. A. Boyko, and S. B. Calderwood.** 1992. Cloning, sequencing, and transcriptional regulation of the *Vibrio cholerae fur* gene. J. Bacteriol. **174:**1897–1903.
29. **Macomber, L., and J. A. Imlay.** 2009. The iron-sulfur clusters of dehydratases are primary intracellular targets of copper toxicity. Proc. Natl. Acad. Sci. U. S. A. **106:**8344–8349.
30. **Messner, K. R., and J. A. Imlay.** 2002. Mechanism of superoxide and hydrogen peroxide formation by fumarate reductase, succinate dehydrogenase, and aspartate oxidase. J. Biol. Chem. **277:**42563–42571.
31. **Messner, K. R., and J. A. Imlay.** 1999. The identification of primary sites of superoxide and hydrogen peroxide formation in the aerobic respiratory chain and sulfite reductase complex of Escherichia coli. J. Biol. Chem. **274:**10119–10128.
32. **Nordlie, R. C., and W. J. Arion.** 1966. Glucose-6-phosphatase. Methods Enzymol. **9:**619–625.
33. **Rice, K. C., and K. W. Bayles.** 2003. Death's toolbox: examining the molecular components of bacterial programmed cell death. Mol. Microbiol. **50:** 729–738.
34. **Rice, K. C., B. A. Firek, J. B. Nelson, S. J. Yang, T. G. Patton, and K. W. Bayles.** 2003. The *Staphylococcus aureus cidAB* operon: evaluation of its role in regulation of murein hydrolase activity and penicillin tolerance. J. Bacteriol. **185:**2635–2643.
35. **Robin, A. Y., and K. M. Fromm.** 2006. Coordination polymer networks with O- and N-donors: what they are, why and how they are made. Coord. Chem. Rev. **250:**2127–2157.
36. **Robin, A. Y., M. Meuwly, K. M. Fromm, H. Goesmann, and G. Bernardinelli.** 2004. How many structures are there for $\{[AgL](NO_3)(H_2O)n\}$? Water-content dependent variations in the structure of $\{[AgL](NO_3)(H_2O)n\}$, n = 0, 1, 2; L = ethanediyl bis(isonicotinate). CrystEngComm **6:**336–343.
37. **Robin, A. Y., J. L. Sague, and K. M. Fromm.** 2006. On the coordination behaviour of NO_3^- in coordination compounds with Ag^+. Part 1. Solubility effect on the formation of coordination polymer networks between $AgNO_3$ and L [L = ethanediyl bis(isonicotinate)] as a function of solvent. CrystEngComm **8**(5)**:**403–416.
38. **Robin, A. Y., J. L. Sague Doimeadios, A. Neels, T. Vig Slenters, and K. M. Fromm.** 2007. Structure-property relationships: polymorphism, solvates, and clay behavior in the one-dimensional coordination polymer chains $[Ag(L)(NO_3)](H_2O)n$, L = ethanediyl bis(isonicotinate), n = 0, and 2. Inorg. Chim. Acta **360:**212–220.

39. **Rohde, H., E. C. Burandt, N. Siemssen, L. Frommelt, C. Burdelski, S. Wurster, S. Scherpe, A. P. Davies, L. G. Harris, M. A. Horstkotte, J. K. Knobloch, C. Ragunath, J. B. Kaplan, and D. Mack.** 2007. Polysaccharide intercellular adhesin or protein factors in biofilm accumulation of Staphylococcus epidermidis and Staphylococcus aureus isolated from prosthetic hip and knee joint infections. Biomaterials **28:**1711–1720.
40. **Sadykov, M. R., M. E. Olson, S. Halouska, Y. Zhu, P. D. Fey, R. Powers, and G. A. Somerville.** 2008. Tricarboxylic acid cycle-dependent regulation of *Staphylococcus epidermidis* polysaccharide intercellular adhesin synthesis. J. Bacteriol. **190:**7621–7632.
41. **Setsukinai, K., Y. Urano, K. Kakinuma, H. J. Majima, and T. Nagano.** 2003. Development of novel fluorescence probes that can reliably detect reactive oxygen species and distinguish specific species. J. Biol. Chem. **278:**3170–3175.
42. **Slenters, T. V., I. Hauser-Gerspach, A. U. Daniels, and K. M. Fromm.** 2008. Silver coordination compounds as light-stable, nano-structured and antibacterial coatings for dental implant and restorative materials. J. Mater. Chem. **18:**5359–5362.
43. **Somerville, G. A., and R. A. Proctor.** 2009. At the crossroads of bacterial metabolism and virulence factor synthesis in staphylococci. Microbiol. Mol. Biol. Rev. **73:**233–248.
44. **Spadaro, J. A., T. J. Berger, S. D. Barranco, S. E. Chapin, and R. O. Becker.** 1974. Antibacterial effects of silver electrodes with weak direct current. Antimicrob. Agents Chemother. **6:**637–642.
45. **von Eiff, C., G. Peters, and C. Heilmann.** 2002. Pathogenesis of infections due to coagulase-negative staphylococci. Lancet Infect. Dis. **2:**677–685.
46. **Yamanaka, M., K. Hara, and J. Kudo.** 2005. Bactericidal actions of a silver ion solution on *Escherichia coli*, studied by energy-filtering transmission electron microscopy and proteomic analysis. Appl. Environ. Microbiol. **71:**7589–7593.
47. **Yao, Y., D. E. Sturdevant, and M. Otto.** 2005. Genomewide analysis of gene expression in Staphylococcus epidermidis biofilms: insights into the pathophysiology of S. epidermidis biofilms and the role of phenol-soluble modulins in formation of biofilms. J. Infect. Dis. **191:**289–298.
48. **Zhang, Y. Q., S. X. Ren, H. L. Li, Y. X. Wang, G. Fu, J. Yang, Z. Q. Qin, Y. G. Miao, W. Y. Wang, R. S. Chen, Y. Shen, Z. Chen, Z. H. Yuan, G. P. Zhao, D. Qu, A. Danchin, and Y. M. Wen.** 2003. Genome-based analysis of virulence genes in a non-biofilm-forming Staphylococcus epidermidis strain (ATCC 12228). Mol. Microbiol. **49:**1577–1593.
49. **Zimmerli, W.** 1999. Tissue cage infection model, p. 409–417. *In* O. Zak and M. A. Sande (ed.), Handbook of animal models of infection. Academic Press, London, United Kingdom.
50. **Zimmerli, W., A. Trampuz, and P. E. Ochsner.** 2004. Prosthetic-joint infections. N. Engl. J. Med. **351:**1645–1654.